Graphical Abstract

Characterizing Mangrove Forest Succession in Suriname using GEDI waveform metrics

Jasper Feyen, Frieke Vancoillie, Verginia Wortel, Kim Calders, John Armston

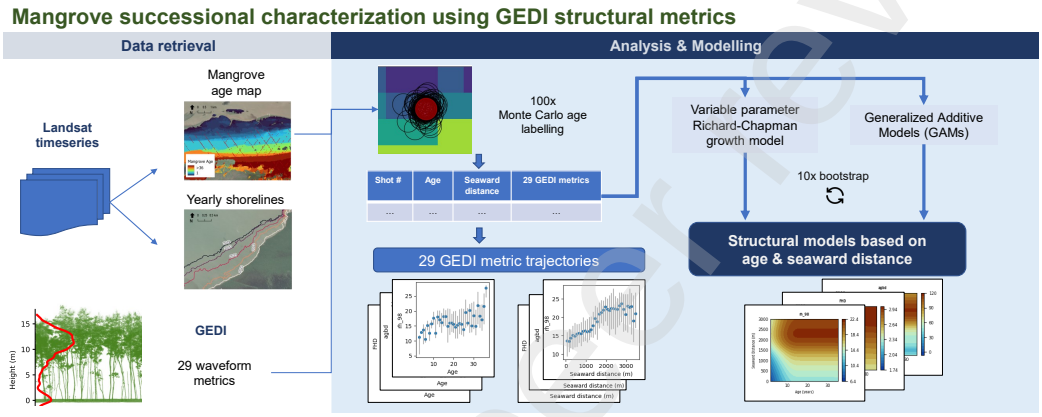

Highlights

Characterizing Mangrove Forest Succession in Suriname using GEDI waveform metrics

Jasper Feyen, Frieke Vancoillie, Verginia Wortel, Kim Calders, John Armston

- Integrated stand age and seaward distance to characterize mangrove succession using GEDI metrics.
- GEDI shot data effectively captured mangrove successional characteristics across temporal and spatial gradients.
- Non-linear models and GAMs revealed growth and complexity patterns in mangrove ecosystems.
- Age and seaward distance jointly shape mangrove structural traits
- Study highlights GEDI's potential for monitoring mangrove successional stages and dynamics.

Characterizing Mangrove Forest Succession in Suriname using GEDI waveform metrics

Jasper Feyen[a], Frieke Vancoillie[a], Verginia Wortel[b], Kim Calders[a], John Armston[c]

[a] *Q-ForestLab - Laboratory of Quantitative Forest Ecosystem Science, Department of Environment, Ghent University, Belgium*
[b] *Department of Forest Management, Centre for Agricultural Research in Suriname (CELOS), Paramaribo, Suriname*
[c] *Department of Geographical Sciences, University of Maryland, United States*

Abstract

Mangroves are critical coastal ecosystems known for their carbon storage capacity, biodiversity, and shoreline stabilization. In Suriname, mangroves develop within a dynamic environment shaped by migrating mudbanks. In this study we examined how 29 structural metrics derived from the Global Ecosystem Dynamics Investigtation (GEDI) vary across gradients of mangrove stand age and seaward distance. Forest stand age and yearly coastlines were derived from Landsat time series, enabling the integration of temporal and spatial drivers to uncover patterns of mangrove succession and structure. Non-linear models, including the Chapman-Richards growth function, captured early growth and stabilization phases, while Generalized Additive Models (GAMs) provided flexibility to model more complex structural changes, particularly in mature and decaying mangrove stands. Results show that forest growth metrics like canopy height and biomass increase rapidly during early successional stages but plateau beyond 12 years or 2 km from the coastline. Complexity-oriented metrics, such as Foliage Height Diver-

sity (FHD) and the Waveform Structural Complexity Index (WSCI), however continue to evolve, reflecting increased vertical stratification in mature stands. By combining high-resolution GEDI LiDAR data with Landsat time series, this study demonstrates the possible use of GEDI spaceborne LiDAR data for monitoring mangrove successional trajectories and structural complexity. Our findings contribute to advancing remote sensing approaches for long-term mangrove ecosystem monitoring, emphasizing the combined effects of age and environmental gradients on mangrove structure.
Keywords: mangroves, GEDI, waveform lidar, gam, forest structure, succession, biomass, growth modelling, generative additive models, chronosequences

1. Introduction

Mangroves are among the most carbon-dense ecosystems globally, playing a critical role in carbon storage, coastal protection, and biodiversity support (**??**). Known as the "nurseries of the seas", they provide vital habitats for numerous marine and avian species (**?**). In Suriname, mangroves extend over 350 km along the coastline and ocean-bound river shores, forming part of the Guiana Shield mangrove system, which spans from Brazil to Venezuela. Unlike the diverse mangrove ecosystems in Southeast Asia, Suriname's mangrove forests are species-poor, dominated by *Avicennia germinans* along the coast and *Rhizophora mangle* near riverbanks (**??**).

The development of the Guianese mangroves is tightly linked to the dynamic coastal system of migrating mudbanks originating from the Amazon River. These mudbanks are transported westward by coastal currents along

the Guianese coastline to the Orinoco Delta in Venezuela at an average speed of 2 km per year (**?????**). Trade winds and the 18.6-year tidal cycle shape these mudbanks, causing alternating periods of rapid coastal accretion and erosion (**???**).

With an arriving mudbank, new sediments are deposited along the coastline and enhances wave damping, which facilitates the colonization of pioneer mangrove species, predominantly *Avicennia germinans*, often accompanied by *Laguncularia racemosa* (**??**). Although not completely understood, ideal colonization conditions result from a balance between sediment fluxes, wave and wind conditions, and tidal elevation (**??**). Pioneer stands further stabilize the mudbanks, leading to additional mud deposition and wave attenuation (**?**). Mudbank topography plays a significant role, with colonization occurring predominantly between the Mean Water Level (MWL) and Mean High Water Level (MHWL), particularly in areas where sea currents are relatively weak. Moreover, 'mud cracks' capture opportunistic mangrove propagules, facilitating rapid colonization (**?**). **?** estimated an average coastal accretion rate of 32 m per year during mudbank presence and an erosion rate of 4 m per year during mudbank absence between 1986 and 2020.

The migrating mudbanks influence the structural and successional properties of mangrove stands, which are both time- and space-dependent. Their distribution and dynamics are primarily controlled by tidal currents, sediment dynamics, and climatic factors (**??**). Mangrove development is often studied through two major perspectives: age and seaward distance. Several studies have focused on age as a key determinant of structural progression and biomass accumulation in mangroves (**????**). Others use the distance

between the seafront and the mangrove stand, following environmental gradients such as salinity and tidal influence (**???????**). This also corresponds with the successional mangrove model in French Guiana described by **?** and the evolutionary model developed by **?**, where the relative distance to the seashore were identified as the major parameter for mangrove succession and biomass growth. By integrating both age and seaward distance, this study provides a more nuanced understanding of how mangrove structure responds to these overlapping temporal and spatial drivers. Previous studies quantifying mangrove structural characteristics during different successional stages have largely relied on data collected from a limited number of field plots (**???**). These studies typically focused on a narrow set of structural metrics, such as Diameter at Breast Height (DBH), tree height, and stem density to describe successional stages. While valuable, these traditional metrics provide only a partial view of mangrove structural complexity. More intricate properties, such as crown dimensions, branch architecture, and overall vertical complexity, are challenging to measure manually in the field (**???**). Furthermore, species-specific structural attributes are strongly influenced by biotic and abiotic environmental conditions, yet research exploring these linkages remains limited (**?**). Expanding structural assessments to include these more complex metrics is crucial for capturing the nuanced dynamics of mangrove succession and their interactions with environmental gradients. However, regional monitoring faces challenges due to the inaccessibility of mangroves and the time and cost of comprehensive spatio-temporal sampling.

Optical remote sensing has provided valuable tools for large-scale forest

monitoring, but traditional methods lacked vertical structural detail. Recent advances, such as GEDI, address this limitation by providing global, high-resolution LiDAR data on forest structure (**?**).

Light Detection and Ranging (LiDAR), an active remote sensing technique, provides crucial information on vertical forest structure (**?**). LiDAR instruments such as Terrestrial and Aerial Laser Scanners offer high-resolution vertical data over large areas. However, their use requires expensive equipment and proximity to the area of interest, which limits their application for larger-scale regional structural monitoring and assessment. In 2018, the Global Ecosystem Dynamics Investigation (GEDI) was launched to the International Space Station (ISS) by NASA. GEDI is a waveform recording satellite laser altimeter collecting vegetation structure data on a global and systematic scale (**?**). Each shot covers a 25m footprint, providing structural metrics such as canopy height and aboveground biomass density (**?**). Recent studies successfully used GEDI data for assessing forest growth rates: (**?**) used GEDI and ICESAT-2 data collected over a chronosequence to obtain forest regrowth rates in the amazon rainforest. (**?**) assessed forest recovery rates by fusing GEDI data with the Annual Forest Change classification map of Brazil. **?** used GEDI for assessing forest dynamics in a fast-growing forest in Spain.

This study leverages GEDI-derived structural metrics and Suriname's unique chronosequences to explore how mangrove structure responds to temporal and spatial gradients. Specifically, we aim to:

1. Investigate how mangrove structural traits, derived from GEDI lidar data, vary across a gradient of stand ages and seaward distance introduced.

2. Evaluate the effectiveness of nonlinear growth functions and Generalized Additive Models (GAMs) in capturing the combined influence of stand age and seaward distance on mangrove structure.

With this study we aim to identify the potential use of spaceborne LiDAR data for monitoring mangrove successional stages to support long-term ecosystem observation.

2. Study Area

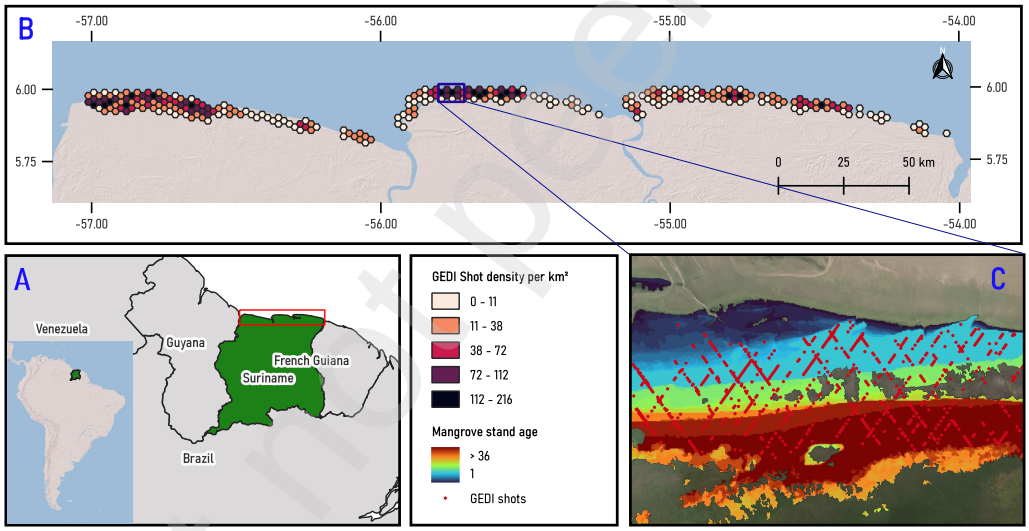

Figure 1: A) Overview map of the study area in Suriname. Hexagons in B show the number of GEDI shots per 5 km² cell, within the coastal mangrove ecosystem, dominated by *Avicennia germinans*. C) illustrates the GEDI sampling traject over the mangroves, coloured by estimated mangrove stand age.

The study area encompasses the entire mangrove forest zone of Suriname (figure 1), which stretches along the coast and the upper shores of the larger

rivers and comprises $\sim$ 876 km^2 in 2023. The mangrove ecosystem in Suriname exhibits relatively low species diversity, only dominated by three mangrove species. *Avicennia germinans* (black mangrove) is the most abundant, covering $\sim$ 548 km^2 (67%) of the mangrove area. It forms monospecific and homogeneous stands along the coastal fringe, and is well-adapted to saline conditions with its aerial pneumatophores facilitating gas exchange in waterlogged soils. *Avicennia germinans* (black mangrove) is the most abundant, occupying approximately 548 km^2 (67%) of the mangrove area. It forms monospecific and homogeneous stands along the coastal fringe and is well adapted to saline conditions, with aerial pneumatophores that facilitate gas exchange in waterlogged soils. *Rhizophora mangle* (red mangrove) dominates inland riverbanks, particularly where freshwater inflow dilutes salinity, covering around 273 km^2 (33%) of the mangrove zone. Although other mangrove species such as *Rhizophora racemosa* and *Rhizophora harrizonii* are also present in the study area, they occur less frequently and are typically found in mixed stands with the dominant species (**?**). A third mangrove species, *Laguncularia racemosa* (white mangrove) can be found as small patches in the brackish areas within the *Rhizophora* belts and is adapted to tolerate varying salinity levels and can thrive in environments where freshwater influence is more pronounced. The region has a semi-diurnal micro-tidal regime with two high and two low tides per day, with a spring tide of $\sim$2.5 m and a mean tidal range of $\sim$1.8 m (**?**). This micro-tidal system ensures that the pneumatophores of coastal *Avicennia* stands are rarely fully submerged.

Mangrove succession in the region follows a well-defined trajectory, as described by **?** in French Guiana. Newly colonized stands stabilize mudbanks

over time, transitioning through even-aged successional stages: pioneering, young, adult, mature, and mixed stands. These stages align with the "self-thinning rule" of **?**, forming natural chronosequences along a north-south transect as stands mature and grow further inland (**??**). With an increasing seaward distance, mudbank stabilization reduces tidal flooding, creating less saline and more freshwater-dominated conditions (**??**). However, in poorly drained zones, salinity stress may lead to large-scale die-offs, resulting in so-called "cemetery stands".

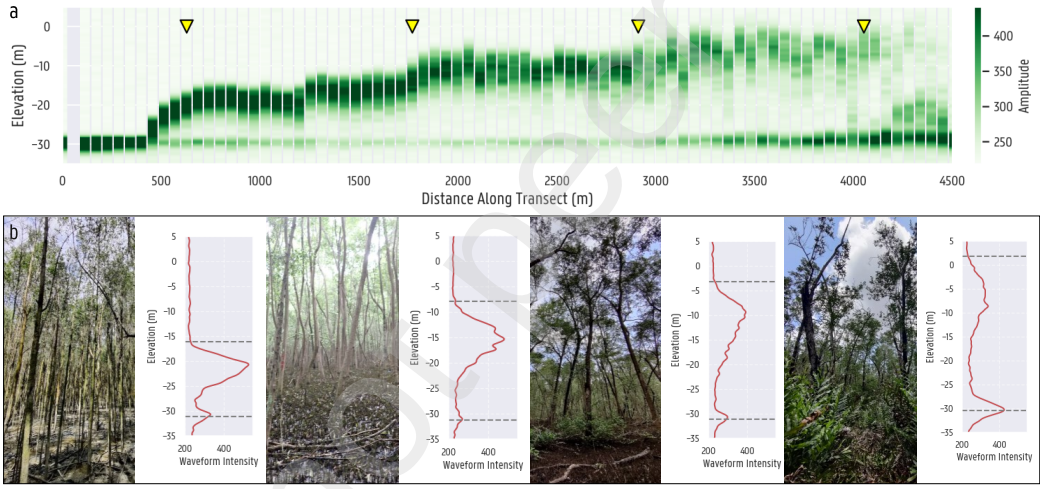

Figure 2: a) Elevation profile along a sample GEDI transect. Elevation is measured by GEDI as relative to a sample ellipsoid. b) Sample GEDI waveforms from the locations along the transect indicated with the yellow marks.

3. Methods

3.1. Age mapping using Landsat data

To analyze the temporal development of mangrove ecosystems, annual maps of mangrove cover were generated using Landsat multispectral data

processed in Google Earth Engine (GEE) (**?**). This approach enabled us to track changes in mangrove distribution from 1988 to 2024. The full Landsat archive was used to produce cloud-free image mosaics for each year, focusing on the broader dry season (May to November) to ensure consistent data quality and minimize seasonal variability. Preprocessing steps included cloud and shadow masking, followed by the application of a geometric median reducer to reduce noise and outliers, ensuring robust data quality (**?**). The resulting composites were classified using a random forest classifier, chosen for its accuracy and ability to handle complex relationships in heterogeneous land cover data (**?**). The outputs from this method provided a consistent time series of yearly mangrove cover maps, which were then used to derive mangrove stand ages by tracking the first year of continuous mangrove detection for each pixel. Full details on this methodology, including the temporal and spatial filters applied to the yearly classifications and the algorithm used for mangrove age mapping, are available in Supplementary A.

3.2. GEDI data for structural assessment of mangrove stands

3.2.1. GEDI preprocessing

GEDI Level 1B, 2A, 2B, 4A, and 4C data were collected for the period 2019–2023 (**????**). Metrics in the 2A and 2B products are derived from 1B waveforms using six algorithm setting groups with varying background noise thresholds (**?**). The version 2 dataset used in this study automatically selects the optimal algorithm and Gaussian smoothing widths, though alternative settings remain available. Figure 2 shows an example GEDI transect over the illustrated study area in figure 1 C.

To ensure high-quality data, multiple filters were applied to the GEDI shots:

- Only shots with Level 2A and 2B quality flags set to 1 were retained, as these flags relate to the quality of a shot based on the sensing conditions and registered laser return (**?**).
- Each shot was buffered with a 25 m radius and compared to annual mangrove cover maps to ensure it fell entirely within the *Avicenia germinans* dominated area. Shots were excluded if any of the pixels within the buffer were classified as non-mangrove.
- A minimum sensitivity threshold - calculated from the a2 setting group for all shots - of 0.95 was applied. The sensitivity reflects the maximum canopy cover penetration achievable under the signal-to-noise ratio of the waveform and thus represents the ability to detect the ground. While some studies recommend a higher sensitivity threshold of 0.97 (**?**) or 0.98 (**?**) for shots in dense forests,a threshold of 0.95 was selected to balance data quality and retention (**??**).
- A spatial filter was applied following **?**, combining a 1D Extended Local Minimum (ELM) and a Progressive Morphological Filter (PMF) along each transect: first, ELM (cell size = 200 m; depth threshold = 4 m) flagged and removed isolated dips in the profile; then the PMF (max_window_size = 10 000 m; slope = 0.0012; initial_distance = 0.2 m; max_distance = 12 m) classified the remaining points as ground (class 2) or canopy (class 1), thus excluding deep outliers and canopy

artefacts while preserving the flat surface morphology (Supplementary B).

Potential uncertainties in GEDI metrics, such as tidal flooding and terrain slope, were also evaluated. Tidal sub-canopy conditions, especially during spring tides, can affect tree height estimates (**?**). However, given Suriname's micro-tidal regime, this effect was deemed negligible. The flat terrain of the study area also minimized slope-related biases in elevation and height metrics, consistent with previous findings (**??**). Nevertheless, further investigation into the local effects of the tidal regime could help assess this uncertainty at different scales.

3.2.2. GEDI metric extraction

Waveform derived metrics

A total of 28 GEDI metrics were derived (Table 1). The raw geolocated metrics from the L1B product were utilized to calculate several supplementary metrics using the *waveformLidar* package by **?** in R. These metrics include the number of waveform peaks ($npeaks$), The proportion of vegetation and ground area (V_int, G_int, The ratio of vegetation to ground proportion ($RtVG$), The distance from waveform beginning to the first peak, indicating the roughness of the outermost canopy ($ROUGH$), The angle from waveform beginning to the first peak, known as Front Slope (FS). Furthermore, the centroid coordinates (Cx, Cy) and the radius of Gyration (RG) were calculated, contributing additional shape-based metrics. These additional shape-based metrics capture structural variability not represented in height-based metrics (**?**)). The GEDI Level 2A product includes relative height

(rh) metrics, which characterize the cumulative return energy distribution from the ground ($rh0$) to the tallest canopy point ($rh100$). A linear regression model between the rh-values and the square root of their corresponding height percentiles (0–100), following the method proposed by **?**). This approach resulted in three derived metrics from the regression model:

1. the slope of the linear model ($coef\_slope$) reflecting the vertical distribution rate,
2. the intercept of the model ($coef\_int$)
3. The residual variance ($rsdvar$), which captures the variability not explained by the linear fit.

In addition to these regression-based metrics, we retained key rh-values ($rh5, rh25, rh50, rh75$, and $rh98$) to represent specific canopy height percentiles. The $rh98$ metric corresponds to canopy height, providing a direct measure of stand height. A canopy height ratio was also calculated based on the relative height metrics to further quantify vertical canopy structure. The Level-2B data contains extracted biophysical metrics from each waveform, based on the directional gap probability profile derived from the L1B waveform (**?**), such as the Plant Area Index (PAI), Plant Area Volume Density ($PAVD$) and the Foliage Height Diversity (FHD).

Above ground biomass density

The GEDI level 4A contains footprint-level the aboveground biomass density ($agbd$) derived using region-specific allometric models and plant functional types (**?**). For Suriname, biomass estimates were calculated using the allometric model designed for Evergreen Broadleaf Trees (EBT) in South

Table 1: Extracted GEDI metrics used to characterize the mangrove forest in Suriname

	GEDI products + derivatives from LPDAAC				
	L1B Geolocated waveforms	**L2A** Relative Height Metrics	**L2B** Extracted biopsychical metrics	**L4A** *agbd*	**L4C** ***WSCI***
Method	Waveform metrics with R-package waveform lidar (Zhou & Popescu, 2018).	Summarizing 101 rh metrics (Diwuptra et al., 2022): $\text{rh}_x \sim \sqrt{x},\ x \in [0, 100]$ Slope coëfficiënt ($coef\_slope$) Intercept coefficiënt ($coef\_int$)	Canopy Cover and Vertical Profile Metrics	AGB density values from regional models by Duncanson et al. (2021)	Waveform Structural Complexity Index (by de Conto et al., 2024)
Metrics	Slope (FS) *Rough* *npeaks* V_int Vegetation area G_int: Ground area $RtVG$: Ratio Vegetation/Ground Cx, Cy, Radius of Gyration (RG) $HOHE$, $HEHR$	$coef\_slope$ $coef\_int$ $rsdvar$ $rh25$ $rh50$ $rh75$ $rh98$ (Canopy Height)	Plant Area Index (PAI) *cover* Foliage Height Diversity (FHD) $PAI_{0\text{–}10m}$ $PAI_{10\text{–}20m}$	agbd ($Mg.ha^{-1}$)	$WSCI$ $WSCI_{xy}$ $WSCI_z$

America. This model utilizes the 50th and 98th relative height metrics as key predictors of forest biomass. This model is developed by using a total of 3441 simulated waveforms derived from colocated field plot inventory and ALS data with a reported R^2 of 0.66.

$$\text{agbd} = 1.106 \times \Big(-134.770 + 6.654\sqrt{\text{rh50} + 100} + 6.687\big(\sqrt{\text{rh98} + 100}\big)^2 \Big) \tag{1}$$

To account for model uncertainty, prediction errors were propagated using 100 Monte Carlo simulations for each GEDI footprint. Biomass density (agbd_i) was modeled as:

$$\text{agbd}_i = \text{agbd}_{\text{pred}} + \varepsilon, \quad \varepsilon \sim \mathcal{N}(0, \text{agbd}_{\text{SE}}) \tag{2}$$

where $\text{agbd}_{\text{pred}}$ represents the predicted biomass value, and agbd_{SE} is the standard error associated with the prediction. This approach allowed

for robust error estimation and provided a more reliable representation of biomass uncertainty across the study area.

Waveform Structural Complexity Index ($WSCI$)

The Waveform Structural Complexity Index ($WSCI$) was derived from GEDI Level 4C data (**?**). The $WSCI$ is a valuable metric for assessing the three-dimensional structural complexity of forest canopies, as it incorporates both horizontal and vertical structural components. This index assesses three-dimensional canopy structural complexity by integrating both horizontal and vertical components. Unlike Foliage Height Diversity (FHD), which focuses solely on vertical structure, $WSCI$ provides a more comprehensive assessment by incorporating horizontal variability. The $WSCI$ is derived by modeling the relationship between high-resolution Airborne Laser Scanning (ALS) derived 3D structural complexity and GEDI's relative height (RH) metrics using XGBoost.

3.2.3. Geolocation uncertainty & Age labeling

When fusing the GEDI data with age maps, geolocation uncertainty should be addressed to ensure accurate analyses (**?**). The GEDI samples have a reported average horizontal geolocation error of 10 m (1σ) in their 25 m diameter footprints (**?**). This geolocation error can introduce substantial prediction errors, particularly in heterogeneous canopies such as fragmented mangrove stands and inland mangrove edges, where a GEDI shot may only partially capture the mangrove area.

To account for this, a Monte Carlo approach, as proposed by **?** and **?**, was implemented to propagate both geolocation and age-related uncertainties.

During the Monte Carlo simulations, 100 random geolocation errors were generated for each GEDI shot. The new coordinates for each simulation were calculated as:

$$X = x_i + r_i \cos(\theta_i) \tag{3}$$

$$Y = y_i + r_i \sin(\theta_i) \tag{4}$$

where r_i is the geolocation error for simulation i, sampled from a normal distribution $r_i \sim \mathcal{N}(0, 10.2)$, and θ_i is a random angle sampled from a uniform distribution $\theta_i \sim U(0, 360)$.

For each simulated location, an overlay operation was performed with the age map corresponding to the acquisition year of the GEDI shot (Figure 2). The standard deviation of mangrove age across the 100 simulations was calculated for each shot. Shots with a standard deviation exceeding a threshold of 2 years were excluded from the dataset. This threshold minimizes errors from highly variable geolocation adjustments while retaining sufficient data for analysis (**?**).

Additional filters were applied to improve data reliability. Shots with an estimated median age below 2 years were excluded, as age estimations are performed on an annual basis, making measurements for younger ages unreliable.

After applying all filters, a final collection of 9338 shots within the *Avicennia germinans* dominated mangrove ecosystem was retained for further processing. Together with the 100 simulated *agbd* values, a total of 100 Monte Carlo age-agbd sets per shot were used for further modelling and variability assessment.

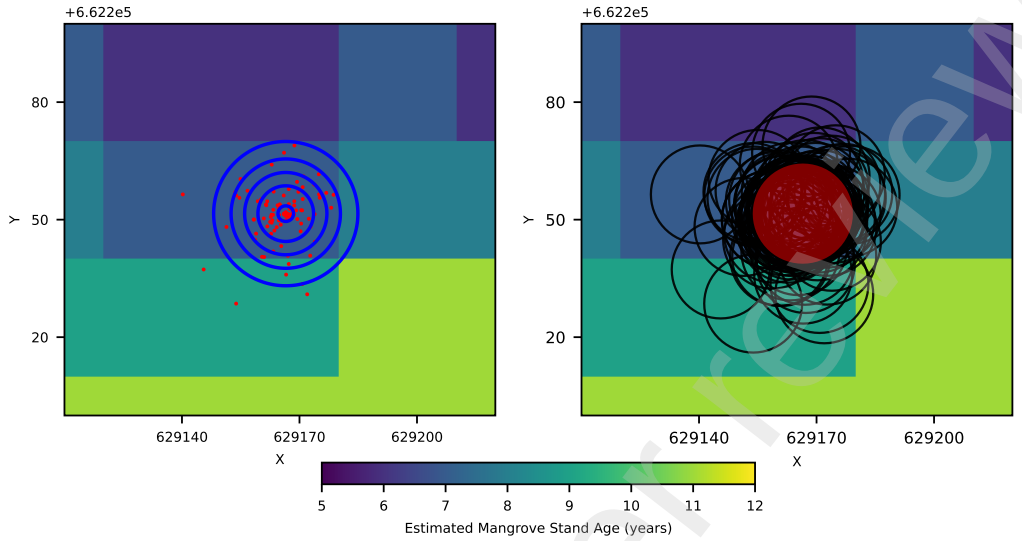

Figure 3: Illustration of the geolocation error of a GEDI footprint on a 20x20 Mangrove stand age map. a) 100 Simulated GEDI center points. The blue circles are the 2D gaussian contours. Right: The red circle is the reported location of the GEDI shot with it's 25m diameter, the black circles show the shited 25m footprints on the GEDI Age Map.

3.3. Coastline detection and seaward distance

For 2019 – 2023, the years where GEDI shots were available, the coastline was extracted using the Automatic Water Extraction index (AWEI) on the annual Landsat mosaics with Otsu thresholding in Google Earth Engine (**?**). Small inland water bodies and islands were removed, using a script adapted from **?**. The resulting vector files were manually inspected and refined in QGIS to ensure the accuracy of the coastal boundaries, leaving only the shorelines associated with the coastal area. Based on the detected shorelines for 2019 – 2023, the Euclidean seaward distance from the center of each GEDI shot footprint to the nearest point on the detected coastline was calculated using the GeoPandas package. (**?**). Finally, the calculated distances were

categorized into 200 m bins to facilitate analysis along the seaward gradient.

3.4. Statistical assessment of the effect of age and seaward distance on mangrove structural traits

In the initial statistical analysis we examined the correlation between each of the GEDI structural metrics and the estimated mangrove age and seaward distance using Kendall's Tau coefficient. Kendall's Tau coefficient was selected as the correlation measure due to its robustness against outliers and its suitability for non-parametric data since it does not require assumptions on the data distribution (**?**). This is particularly important because the structural characteristics of mangroves derived from GEDI data may not follow a normal distribution (Supplementary F). To evaluate whether each GEDI metric was more strongly correlated with age or seaward distance, we applied Zou's method for comparing dependent correlation coefficients (**?**). This approach accounts for the shared dependency of data pairs when calculating the difference between correlations. Confidence intervals were constructed for the difference between the two correlations. If this interval includes zero, this indicates that there is no statistically significant difference between the correlation of a given metric with age versus seaward distance. By assessing each GEDI metric in this way, we aim to clarify which predictor—age or seaward distance—has a more pronounced association with mangrove structural variation. The results form the foundation for subsequent modeling efforts, aimed at disentangling the combined effects of temporal and spatial gradients on mangrove structural traits.

3.5. Modelling mangrove successional development

3.5.1. Aggregation of GEDI data

All GEDI shots were aggregated based on both age and seaward distance and the median values for agbd and rh98 were calculated for each age-seaward distance group. By using the median, we ensure that extreme values do not disproportionately influence the group-level estimates, leading to a more representative summary of mangrove structure for each age–distance group. To ensure there was no multicollinearity between mangrove age and seaward distance, the Variance Inflation Factor (VIF) was calculated. High VIF values (¿ 5) indicate that both variables are multicollinear, which can lead to unstable estimates and reduced interpretability. The VIF values for both the grouped data as the original GEDI data set were both less than 5 (table S2, Supplementary D), ensuring that both variables could be included in the models.

3.5.2. Nonlinear modelling of mangrove stand growth

Four different types of non-linear growth functions were considered to model canopy height (*rh98*) and aboveground biomass density (*agbd*) as these metrics are frequently used to establish nonlinear relationships for forest growth (**?**). After fitting these functions to the aggregated data (Supplementary E), the Chapman-Richards model was selected due to its flexibility and the biological interpretability of its parameters (**?**). The Chapman-Richards model, a generalization of von Bertalanffy's growth model, is widely applied in forest growth studies and is expressed as:

$$f(x) = A\left(1 - e^{-k \cdot \text{age}}\right)^{m} \tag{5}$$

where $f(x)$ represents the growth metric (biomass density or canopy height), A is the asymptotic value (maximum possible growth), k is the growth rate, and m is the shape parameter that modifies the curvature of the growth trajectory.

To account for the effects of environmental heterogeneity on mangrove structure, seaward distance (SD) was introduced as an explanatory variable. Visual inspection of scatter plots 4 indicated that a linear relationship between seaward distance and key variables, such as forest height and biomass, was appropriate for distances up to 2000 m. Therefore, the parameters of the Chapman-Richards model were extended to incorporate seaward distance linearly as follows:

$$A = A_0 + A_1 \cdot SD \tag{6}$$

$$k = k_0 + k_1 \cdot SD \tag{7}$$

$$m = m_0 + m_1 \cdot SD \tag{8}$$

where SD represents the seaward distance. Model fitting and optimization were performed using the `curve_fit` function from Python's SciPy library (**?**).

We evaluated two variants of the Chapman-Richards model: one with a fixed shape parameter (m) and another with m allowed to vary. The variable-m model demonstrated better fit statistics, including lower AIC and BIC values, indicating that the added flexibility in m improved the model's ability to capture growth dynamics. The performance of the final models was assessed based on goodness-of-fit and predictive accuracy metrics.

3.5.3. GAM models

While non-linear models are straightforward to capture the growth and plateauing trends in canopy height or agbd, they are less suitable for modeling metrics with more complex patterns, especially in the mature and decaying phase of the mangrove successional trajectory. Applying nonlinear models to these metrics could overcomplicate the analysis without offering additional insight. Instead, Generalized Additive Models (GAMs) were used to capture the potentially complex relationships between these structural traits and environmental variables, offering greater flexibility while avoiding unnecessary constraints.

GAMs are a semi-parametric class of multiple regression models, allowing nonlinear relationships between the response variable and predictor variables. Unlike traditional linear models, GAMs replace the linear components with smooth functions. This approach enables GAMs to capture complex, nonlinear patterns and interactions in the data, while maintaining interpretability (**??**). Another advantage of GAMs is their relaxed assumptions compared to traditional parametric models. Specifically, GAMs do not need to strictly follow assumptions like equal variance of residuals (homoscedasticity) or the normality of predicted values, making them a robust choice for analysing environmental data which often exhibit variability and uncertainty.

The general GAM structure is expressed as:

$$Y = \beta_0 + s(\text{Age}) + s(\text{Distance}) \tag{9}$$

where Y is the response variable of the exponential family, and $s()$ represents a smooth function applied to the predictors.

GAMs were fitted using the pyGAM package in Python (**?**). During initial data exploration, the most suitable distribution (Normal, Gamma, or Inverse Gaussian) was selected for each GEDI metric using the distfit package (**?**). For each metric and its respective distribution, four GAMs were tested, with constraints applied to the smoothing functions to reflect ecological expectations and control overfitting. These constraints allowed the models to capture key relationships while remaining interpretable and ecologically meaningful. Full details on the fitted GAM configurations are provided in Supplementary E and F.

3.5.4. Model uncertainty & evaluation

To address the inherent variability and potential outliers in GEDI data, a bootstrapping approach was employed to improve the robustness of parameter estimation and quantify model uncertainty (**???**). Specifically, we used a wild bootstrapping strategy on the residuals for each of the 100 age-derived structural metrics sets generated through Monte Carlo simulations.

For each metric and its corresponding dataset, the following steps were performed:

1. Fitted an initial model to obtain initial model parameters.
2. Resampled the residuals (r_i) from the initial model with replacement to generate a new set of residuals (r_i^*).
3. Constructed a bootstrapped dataset:

$$Y_i^* = \hat{Y}_i + v_i r_i^*$$

where $\hat{Y}_i$ represents the fitted values from the original model fit, and

v_i is a random multiplier drawn from the standard normal distribution ($v_i \sim N(0, 1)$).

4. The model was refitted using the synthetic dataset ($Y_i^* \sim$ age, SD) and the fitted parameters were stored.

This process resulted in 10 bootstrapped datasets per original set, leading to a total of 100 model parameters per fitted model (10 sets $\times$ 10 bootstraps). All model estimates were then used to derive the 95% confidence interval on the parameters.

Model performance was evaluated using the leave-one-out cross-validation (LOOCV) method, with metrics including Root Mean Square Error (RMSE), Explained deviance (D^2), Generalized Cross-Validation Score (GCV), Akaike's Information Criterion (AIC) and the Bayesian Information Criterion (BIC). Generalized Cross-Validation (GCV) was used as the primary criterion to select the best-fitting model configuration for each metric, as it balances goodness-of-fit and model complexity.

4. Results

Figure 4 illustrates the interquartile ranges (IQRs) of selected GEDI metrics across gradients of stand age and seaward distance. All metrics are provided in Supplementary C. Data for seaward distance were aggregated into 200 m bins for interpretability. Figure 3 gives the Kendall Tau correlation coefficients for the examined structural metrics and indicates the results of Zou's method. Most structural metrics exhibited clear trends with both age and seaward distance, with significant Kendall tau's. For age, metrics

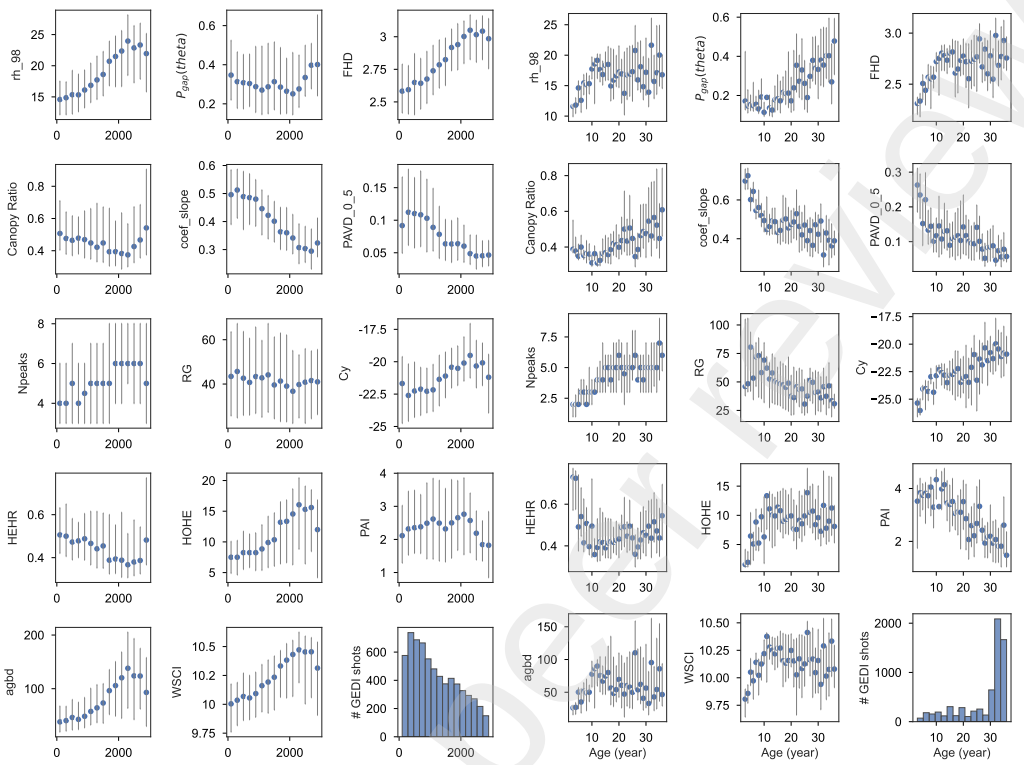

Figure 4: Mangrove transitional patterns across (binned) seaward distance (left) and estimated stand age (right) for selected GEDI-derived metrics. The histogram plots show the number of GEDI shots per seaward distance or age class.

such as rh98 (canopy height) and agbd (aboveground biomass density) increased rapidly during the first 10–15 years, reflecting rapid vertical growth and biomass accumulation, before stabilizing in mature forests. Similarly, with seaward distance, rh98 and agbd increased linearly up to 2–2.5 km, beyond which values plateaued or slightly declined, indicating transitions into decaying mangroves and open swamp zones, characterized by reduced tree height and density. Foliage Height Diversity (FHD), an indicator of vertical stratification, increased consistently with age and peaked at 2 km along

the seaward gradient. Divergent trends were noted for *pgap_theta* – the proportion of gaps in the canopy - which exhibited a positive correlation with age but a slight negative correlation with seaward distance. However, at 2 km, the sudden increase in *pgap_theta* likely reflects decaying forest stands characterized by a higher proportion of broken stems and reduced stem density. Other metrics, such as the slope coefficient (*coef_slope*) and waveform structural complexity index (*WSCI*), displayed continuous increases with age, suggesting progressive structural diversification. For seaward distance, *coef_slope* decreased steadily. Kendall's Tau analysis supported these observations 5. The stronges correlations for seaward distance were found with *FHD*, *coef_slope*, *rh98*, *WSCI*, and *agbd*, while stand age showed stronger correlations with *coef_slope*, the waveform's centroid y-coordinate (*Cy*), and its front slope (*FS*).

4.1. Mangrove growth models

We introduced seaward distance as a linear term in the parameters of the Chapman-Richards growth function (5), resulting in a variable-parameter model. Since the Chapman-Richards growth function is specifically designed to describe the cumulative growth of forest stands over time, models were only fitted for the structural metrics directly related to forest growth: canopy height (rh98) and aboveground biomass density (*agbd*). Parameter estimates and key fitting statistics are provided in Table 2 The model outputs allow estimation of the asymptotic growth accumulation rate (A), the growth rate (k) and shape parameter (m) as a function of seaward distance, offering insights into how mangroves develop across the age and distance gradients.

For both *rh98* and *agbd*, asymptotic accumulation rates (A) increased

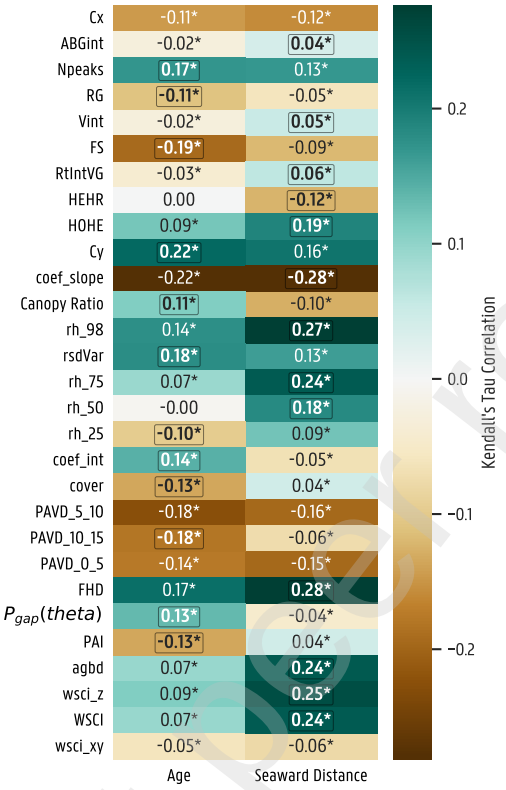

Figure 5: Kendall correlations between Age, Seaward distance to GEDI structural metrics. Asterisks denote statistically significant correlations ($p < 0.05$).The highlighted box marks the predictor (age or seaward distance) with the significantly stronger correlation.

with seaward distance, reflecting greater maximum growth potential in inland mangroves compared to those near the shoreline. Specifically for *agbd*, A ranged from 28.07 Mg ha^{-1} at 0 m to 103.6 Mg ha^{-1} at 2000 m. For *rh98*, A increased from 12.47 m at 0 m to 20.68 m at 2000 m.

The models explained 41% of the deviance in *agbd* (0.41) and 58% of the deviance in *rh98*, with $RMSE$ values of 25.45 Mg ha^{-1} for *agbd* and 2.63 m for *rh98*. These $RMSE$ values correspond to relative uncertainties of 44%

for *agbd* and 17% for rh98, based on their respective mean observed values.

Metric	Adjusted R^2	RMSE	MAE	A (SE)		k (SE)		m (SE)	
agbd (Mg ha^{-1})	0.42	25.72	25.72	A_0	25.5 ± 1.45	k_0	0.40 ± 0.07	m_0	3.94 ± 1.87
				A_1	38.75 ± 1.65	k_1	0.00 ± 0.05	m_1	-0.10 ± 1.72
rh98 (m)	0.56	2.32	1.89	A_0	12.45 ± 1.22	k_0	0.38 ± 0.06	m_0	1.33 ± 0.11
				A_1	4.24 ± 0.51	k_1	-0.04 ± 0.02	m_1	-0.26 ± 0.27

Table 2: Results of the non-linear models with the model parameters, adjusted (R^2), and Root Mean Square Error (RMSE).

4.1.1. Generalized Additive Models (GAM)

Generalized Additive Models (GAMs) were used to analyze the relations between all GEDI-derived structural metrics and the combined effect of mangrove stand and seaward distance. For each metric, multiple constraint settings for age and seaward distance were tested, along with multiple data distributions. Table 3 provides an overview of the selected models with the best GCV score per metric. Key performance metrics such as deviance explained (pseudo R^2) and Root Mean Square Error (RMSE) are reported alongside the constraints applied to age and seaward distance predictors and the chosen distribution for each metric. Figure 6 shows some selected metrics with a contour plot and partial dependence curves for age and seaward distance.

Among all metrics, *coef_slope* showed the highest amount of variation explained (with pseudo $R^2 = 0.75$), followed by Foliage Height Diversity (FHD) and canopy height (*rh98*). For the waveform structural complexity index (wsci), the vertical complexity component (*wsci_z*) had the highest

explained deviance (pseudo-$R^2 = 0.622$) while metrics mostly capturing horizontal structural diversity (*wsci_xy*, *cover*) had lower explained deviances.

The effective degrees of freedom (EDoF) from the GAMs revealed distinct patterns in how mangrove structural metrics respond to age and seaward distance. For most metrics, seaward distance exhibited lower EDF than age, indicating a more linear relationship, likely driven by gradual and predictable environmental gradients. Conversely, age showed higher EDF values for many metrics, reflecting the more complex, non-linear mangrove growth and structural development over time. Interestingly, for metrics such as canopy height (*rh98*) and centroid coordinate (*Cy*), age had a lower EDF than seaward distance, suggesting that these traits are more tightly controlled by temporal growth patterns.

The number of waveform peaks (*Npeaks*) increased steadily over a broad age range, plateauing only after ∼20 years. This indicates continued structural complexity as mangroves mature and accumulate vertical layers.

5. Discussion

5.1. Successional patterns of mangrove structure in relation to age and seaward distance

This study evaluated the potential of GEDI-derived structural metrics to describe successional trajectories in *Avicennia germinans*-dominated mangrove forests in Suriname. Two primary drivers of succession were examined: stand age (temporal driver) and seaward distance (spatial driver). While stand age captures the developmental changes over time, seaward distance acts a proxy for environmental gradients, such as salinity, tidal submersion,

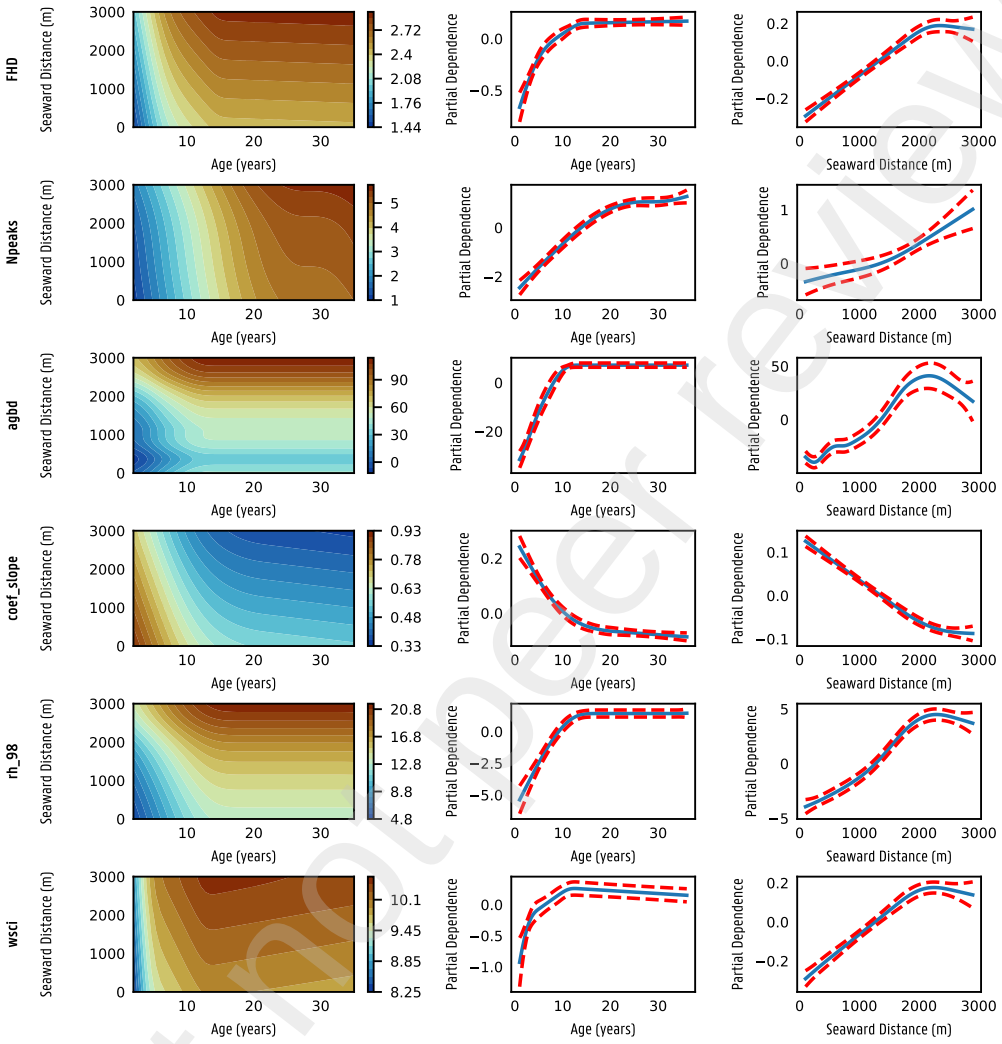

Figure 6: Contour plots and partial dependence curves of the Generalized Additive Models (GAMs) for selected GEDI-derived structural metrics. The blue lines represent the marginal functional estimates of the GAMs, while the red dotted lines indicate the 95% confidence intervals derived from 100 bootstrap samples.

freshwater availability, and sediment deposition (**???**). Patterns in mangrove structure across these gradients highlight both independent and inter-

related effects of age and seaward distance (5). Variance Inflation Factor (VIF) analysis confirmed that these drivers are only moderately correlated, allowing their individual contributions to be examined. Stand age primarily reflects stand growth trajectories, characterized by rapid early development (e.g., height and biomass accumulation) transitioning to stabilization in mature stands. Metrics such as canopy height (*rh98*) and aboveground biomass density (*agbd*) align with these patterns, as do complexity metrics like the number of waveform peaks (*n_peaks*) and *coef_slope*, which increase or decrease with canopy stratification during later stages of development. Seaward distance acts as a proxy for spatial environmental gradients, influencing mangrove structure through reduced tidal stress, stable topography, and nutrient deposition in inland zones reflecting the formation of natural chronosequences driven by mudbank migration. Structural metrics like *rh98*, *agbd*, and FHD increase linearly with distance up to $\tilde{2}$ km before plateauing or declining, reflecting transitions into brackish swamp forests or open swamps. Importantly, seaward distance also interacts with stand age to shape successional patterns. In regions with rapid sediment deposition, such as Coppenamepunt (**?**), mangroves experience accelerated accretion, which supports faster growth and structural complexity. Conversely, in areas with slower sediment dynamics, mangroves exhibit delayed successional development and reduced structural diversity. These findings extend traditional mangrove successional models (**?**), demonstrating how spatial and temporal gradients combine to shape structural trajectories. Metrics like *coef_slope* and FHD capture these dynamics, highlighting the importance of integrating both age and seaward distance to fully understand mangrove development.

5.2. Non-linear models vs GAMs

Seaward distance was introduced into each parameter of the Chapman-Richards growth function (5) for the estimation of canopy height (*rh_98*) and aboveground biomass density (*agbd*). The expected mangrove growth patterns exhibited rapid initial growth, plateauing around 12 years. This pattern aligns with typical mangrove growth trajectories, where stands reach a maturity threshold before height and biomass stabilize. Similarly; mangrove stand height and biomass density also increases with seaward distance up to a distance of 2 km from the shoreline, beyond which growth stabilized or declined. This deceleration corresponds to the transition into brackish swamp forests or open swamps, often characterized by declining tree densities and structural decay. The integration of seaward distance into the Chapman-Richards growth function allowed for the derivation of biologically meaningful parameters (A, k and m). These parameters revealed distinct dynamics: while the asymptotic value A increased linearly with seaward distance, the growth rate (k) slowed, and the shape parameter (m) indicated a more gradual transition to maturity in inland stands. This model is well-suited for the first 2 km but were insufficient for describing structural changes beyond this range, where mangroves transition into the decaying phase. These limitations highlight the need for more flexible modeling approaches to account for complex structural dynamics. Generalized Additive Models (GAMs) addressed these limitations by enabling smooth, non-linear relationships for metrics influenced by both age and seaward distance. GAMs effectively captured diverse trajectories, such as the plateauing of growth metrics like $rh98$ or *agbd* and the continued increase of structural complexity metrics like waveform characteristics as

the number of waveform peaks ($Npeaks$) or the waveform centroid coordinate (Cy) and the extracted biophysical metrics like Foliage Height Diversity (FHD), and the Waveform Structural Complexity Index ($WSCI$). Among vertical complexity metrics, the slope coefficient ($coef\_slope$) emerged as a particularly strong proxy for mangrove succession. This metric, derived from the relative height (rh) metrics, reflects the rate of change in height distribution across the canopy. In younger, homogeneous stands, coef_slope values were steep, reflecting rapid height increases across layers. As stands matured, coef_slope flattened, indicating greater heterogeneity and vertical stratification. A similar trend was observed for Foliage Height Diversity (FHD), which increased with both age and seaward distance, highlighting greater canopy layering and more even foliage distribution in mature stands. The sensitivity of FHD to seaward distance underscores the influence of environmental gradients on vertical structure, likely driven by variations in salinity, tidal submersion, and nutrient availability. The $wsci$ provided additional insights into mangrove structural complexity, particularly its vertical component ($wsci_z$), which correlated strongly with seaward distance. This suggests that environmental gradients play a significant role in shaping vertical structural diversity. In contrast, the horizontal component ($wsci_xy$) showed no significant relationship with age or seaward distance, indicating that vertical layering is more indicative of mangrove successional changes than horizontal spread. Together, these findings suggest that complexity-oriented metrics like coef_slope, FHD, and $WSCI$ provide critical insights into structural dynamics that extend beyond traditional growth metrics. The impact of seaward distance on mangrove structural metrics was further highlighted by the

Waveform Structural Complexity Index ($WSCI$) – a single metric that combines various aspects of canopy structure (Conto et al., 2024). Our analysis indicated that $WSCI$, particularly its vertical component ($wsci_z$), correlates strongly with seaward distance, underscoring the role of environmental conditions in driving structural complexity. The horizontal component ($wsci_{xy}$), however, showed no significant relationship with either age or seaward distance, suggesting that vertical layering rather than horizontal spread is more indicative of mangrove successional changes. Thus, WSCI can also serve as a valuable proxy for structural development, particularly in response to environmental gradients. Our findings contribute to advancing methods for measuring and monitoring mangrove structure at broader scales. While mangrove succession has traditionally been measured through canopy height or biomass, these metrics do not fully capture the complexity of structural development, especially during later successional phases when structural decline or stabilization occurs. Complexity-oriented metrics, such as fhd , rh_slope, $wsci$, and $npeaks$, continue to respond to environmental gradients even after traditional metrics plateau, providing insights into how these factors affect structural properties.

5.3. Limitations and implications for further research

5.3.1. Mangrove age maps

The mangrove stand age maps, derived from Landsat data, are constrained by the spatial resolution (30 m) and temporal extent of available imagery. While these maps effectively capture long-term patterns, they may lack precision in fragmented or heterogeneous mangrove zones. Additionally, the maximum mappable age was capped at 36 years due to Landsat's histor-

ical data availability, potentially grouping older stands into a single category and masking fine-scale successional dynamics.

5.3.2. Model uncertainty & error propagation

GEDI geolocation uncertainty was propagated using Monte Carlo simulations, generating 100 randomized positions for each shot, as recommended by **?** and **?**. This approach accounts for the reported ± 10m horizontal error in GEDI shot placement, reducing the impact of misaligned shots, particularly in heterogeneous landscapes. However, geolocation errors may still contribute to variability in areas with fragmented mangroves or along stand edges, where canopy structure is highly variable. To quantify parameter uncertainty, we applied a wild bootstrapping approach (**?**). This method is well-suited for heteroskedastic data and allowed us to estimate confidence intervals for model parameters, providing robust uncertainty estimates. While wild bootstrapping is not completely immune to spatial autocorrelation effects, it is recommended for models with a spatial dependence structure (**?**). Future studies could explore additional techniques, such as geostatistical resampling, to further account for spatial dependencies in mangrove ecosystems.

6. Conclusion

This study highlights the utility of GEDI-derived structural metrics in improving our understanding of *Avicennia germinans* dominated growth and structural succession across temporal (stand age) and spatial (seaward distance) gradients. By combining these drivers, we characterized structural changes in Suriname's mangrove forests, capturing patterns of development from early growth stages to maturity and eventual decline. Traditional

growth metrics, such as canopy height and aboveground biomass density, followed expected non-linear trajectories, with rapid increases in early stages stabilizing around 12 years of age or $\sim$ 2 km from the seafront. Beyond these thresholds, structural complexity metrics, such as Foliage Height Diversity and the slope coefficient ($coef\_slope$), continued to evolve, offering a more nuanced perspective on structural dynamics even in mature or transitioning stands. GEDI effectively extracted detailed structural metrics, offering insights beyond traditional growth measures. Its ability to quantify vertical complexity provides deeper insights into mangrove successional stages and the effects of environmental gradients. These metrics reveal how mangroves develop more heterogeneous vertical structures as they mature, offering new perspectives on mangrove ecosystem dynamics. Both Chapman-Richards non-linear growth function and Generalized Additive Models (GAMs) were utilized for analyzing these structural traits. The Chapman-Richard function offered biologically meaningful insights into growth rates and asymptotic trends. In contrast, GAMs provided the flexibility to model the complex trajectories of vertical structure, where structural changes extend beyond traditional growth phases. Together, these approaches demonstrated how age and seaward distance influence mangrove structure in complementary ways. This will allow for a better understanding of habitat diversity in mangroves, important for biodiversity conservation. This research expands existing mangrove successional models by integrating growth and vertical complexity metrics. These findings can guide future efforts to map and monitor mangrove structure by combining GEDI-derived metrics with remote sensing data from Sentinel-2, NISAR, BIOMASS, and similar missions, enhancing our ability

to track mangrove dynamics over time.

CRediT authorship contribution statement

JF: Conceptualization, Methodology, Writing - original draft, Visualization, Investigation, Project administration, Software, **FVC**: Conceptualization, Supervision, Writing - review & editing, **KC**: Conceptualization, Supervision, Writing - review & editing, **VW**: Investigation, Writing - review & editing, **JA**: Conceptualization,Writing - review

Acknowledgements

We are thankful to the assistance of the Foundation for Forest Management and Production Control of Suriname (SBB) and the Center for Agricultural Research of Suriname (CELOS) for their valuable insights and accommodation during the field visits in Suriname.

Appendix A. Sample Appendix Section

Table 3: Overview of fitted Generalized Additive Models (GAMs) for each GEDI-derived structural metric. The table presents the explained deviance, Root Mean Square Error (RMSE), constraints applied to the smoother functions for Age and Seaward Distance, and the statistical distribution used for each metric.

Metric	Unit	Adjusted R^2	RMSE	Age		Seaward distance		Distribution
				constraint	edof	constraint	edof	
coef_slope		0.75	0.063	convex	4.4	convex	2.2	gamma
FHD		0.67	0.15	concave	4.9	concave	2.4	normal
rh_98	m	0.67	2.5	monotonic_inc	3.0	None	4.3	normal
wsci_z		0.62	0.15	concave	4.6	concave	2.4	normal
Cy		0.60	22	monotonic_inc	6.7	concave	3.9	normal
wsci		0.57	0.19	concave	5.1	concave	2.7	normal
rh_75	m	0.54	2.8	concave	4.8	concave	1.9	gamma
HOHE	m	0.52	3.1	monotonic_inc	5.5	None	5.2	gamma
Npeaks		0.51	1.2	monotonic_inc	4.1	None	2.0	gamma
agbd	Mg ha^{-1}	0.50	29	monotonic_inc	3.4	None	7.6	gamma
RtIntVG		0.45	0.11	concave	5.8	concave	2.9	normal
PAVD_5_10	m^2/m^3	0.44	0.058	concave	4.1	concave	2.9	gamma
rsdVar		0.44	0.068	convex	7.3	convex	4.7	inv_gauss
FS		0.41	6.0	concave	3.1	concave	2.3	normal
PAVD_0_5	m^2/m^3	0.37	0.046	concave	5.1	concave	1.8	inv_gauss
coef_int		0.37	0.99	convex	5.0	convex	2.9	gamma
Canopy Ratio	m/m	0.35	0.13	convex	7.7	convex	3.0	gamma
HEHR	m	0.34	0.097	convex	6.3	convex	2.1	gamma
cover	%	0.30	0.14	concave	6.1	concave	3.8	normal
Pgap_theta		0.30	0.14	convex	5.7	convex	3.9	gamma
Cx		0.27	17	monotonic_dec	4.0	convex	0.3	gamma
RG		0.22	17	monotonic_dec	3.6	convex	0.4	inv_gauss